Progress in PHOTOVOLTAICS

PROGRESS IN PHOTOVOLTAICS: RESEARCH AND APPLICATIONS
Prog. Photovolt: Res. Appl. (2014)
Published online in Wiley Online Library (wileyonlinelibrary.com). DOI: 10.1002/pip.2510

RESEARCH ARTICLE

Recent progress of high efficiency Si thin-film solar cells in large area

Dong Joo You*, Sun Ho Kim, Hyun Lee, Jin-Won Chung, Sun-Tae Hwang, Youn Ho Heo, Sungeun Lee and Heon-Min Lee

Solar Energy Team, Materials & Components R&D Lab., LG Electronics Advanced Research Institute, Seoul 137-724, Korea

ABSTRACT

Si thin-film solar cells are suitable to the sunbelt region due to a low temperature coefficient and to building integrated photovoltaics owing to flexible size, easily controllable transmittance, and an aesthetic design. Nevertheless, the application is limited until now due to their low conversion efficiency. We have developed a triple junction cell (a-Si:H/a-SiGe:H/μc-Si:H) providing efficient light utilization. For the high efficiency, we have focused on the smoothing of high haze TCO, a low absorption window layer, a low refractive index interlayer, uniformity control of the thickness and crystalline volume fraction in the microcrystalline silicon layer, and a low absorption back reflector. Through these activities, we have achieved a world record of 13.4% stabilized efficiency in the small size cell (1 cm^2) and 10.5% stabilized efficiency in the large area module (1.1 × 1.3 m^2), certificated by the National Renewable Energy Laboratory and Advanced Industrial Science and Technology, respectively. This result was presented in solar cell efficiency tables (Version 41). At this moment, we have increased a stabilized efficiency of 11.2% (Output power 160 W) in the large area module. We will report on the advanced materials in detail for high efficiency. Copyright © 2014 John Wiley & Sons, Ltd.

KEYWORDS

Si thin-film solar cell; large area solar module; TCO smoothing; triple junction; light trapping

***Correspondence**

Dong Joo You, Solar Energy Team, Materials & Components R&D Lab., LG Electronics Advanced Research Institute, Seoul 137-724, Korea.
E-mail: dj.you@lge.com; djryu93@hanmail.net

Received 17 November 2013; Revised 11 February 2014; Accepted 31 March 2014

1. INTRODUCTION

The rate of the implementation of silicon (Si) thin-film solar cells into building integrated photovoltaics (BIPVs) has been gradually increasing owing to the merits of flexible size, easily controllable transmittance, and an aesthetic design [1]. Si thin-film solar cells show high actual power output in a hot climate due to a low temperature coefficient [2,3]. However, Si thin-film solar cells have difficulty in the solar market because the price of crystalline solar cells has been decreasing very dramatically. In order to strengthen the competitiveness of Si thin-film solar cells, a low manufacturing cost ($/W) needs to be provided. Therefore, high-throughput manufacturing equipments for mass production are needed, as well as a reduction in the material cost of glass substrates, process gasses, and modulization materials in order to reduce the cost. In particular, the most important factor is to increase the efficiency of Si thin-film solar cells.

Many groups have adopted multi-absorption layers with various band gaps to efficiently absorb a wide range of wavelengths of light [4–6], in order to improve the conversion efficiency. Recently, B. Yan *et al*. reported a record of initial cell efficiency of 16.3% (by Unisolar) for a triple junction cell with a-Si:H/a-SiGe:H/μc-Si:H absorbing layers [7]. Additionally, we achieved the world record of stabilized cell efficiency of 13.4% (by LG) in a small size (1 cm^2), with a-Si:H/μc-Si:H/μc-Si:H absorbing layers, which was certificated by National Renewable Energy Laboratory [8]. We have tried an a-SiGe:H or μc-Si:H absorbing layer as the middle cell in a large area module. In the case of a-SiGe:H, its thickness is 100–150 nm. While μc-Si:H layer's thickness is about 1 μm. Even though the thickness of the μc-Si:H absorbing layer was 7–10 times the thickness of the a-SiGe:H layer, we had similar stabilized efficiencies in both structures. We cannot but consider the module cost and economics for the commercialization. So we had to choose the triple junction cell

with a-Si:H/a-SiGe:H/μc-Si:H in our pilot line considering the long-term business.

In multi-junction Si thin-film solar cells, the thickness of the amorphous absorbing layers, such as a-Si:H or a-SiGe:H, has to be thin to minimize the impact of light-induced degradation, and its current can limit the current of the device. To overcome this issue, an intermediate layer is introduced between the cells to increase the current of the amorphous cells [9]. For the triple junction (a-Si:H/a-SiGe:H/μc-Si:H) cells, the intermediate layer is introduced between the middle (a-SiGe:H) and bottom (μc-Si:H) cells to compensate for the middle cell current [7]. As the refractive index of the intermediate layer decreases, it can enhance the reflection of the incident light into the top and middle cell. Therefore, we can reduce the thickness of the amorphous absorbing layers in the top and middle cell [10].

Transparent conducting oxide (TCO) plays an important role in light trapping by transmitting and scattering light into the absorption layer [11]. Many research institutes have concentrated on TCO development for a long time to improve the transparency, haze, and electrical conductivity. In view of the optical properties, there have been attempts to increase the transparency of the front TCO to increase the amount of incident light into the absorption layer and to increase the haze to lengthen the effective optical pathlength [12,13]. High haze TCO seems to have a steep morphology, resulting in a shunt path in the device. Regarding the electrical aspects, there have been efforts to improve the electrical conductivity to enable charge carriers to flow more smoothly.

Back reflectors (BRs) should have a high haze property in order to improve the light trapping properties. A BR with high haze sufficiently reflects and scatters light into the absorption layer. In this case, the thickness of the bottom cell (μc-Si:H) can be reduced.

Recently, we achieved the world record in a large area Si thin-film module, which was certificated by Advanced Industrial Science and Technology [8]. We have focused on and developed a high haze TCO substrate, a low absorption doping layer, a low refractive index intermediate layer, a uniform μc-Si:H layer, a high haze and low absorption BR, and module technologies for high efficiency. We present these technologies in detail.

2. EXPERIMENTAL

Large area ($1.1 \times 1.3\ m^2$) Si thin-film solar modules with three absorbing layers (a-Si:H/a-SiGe:H/μc-Si:H) were fabricated. Si-based layers are deposited by mixing H_2, SiH_4, GeH_4 (10 wt.% diluted by H_2 gas), PH_3 (5 wt.% diluted by H_2 gas), CH_4, and CO_2 gasses in the capacitively coupled radio-frequency plasma-enhanced chemical vapor deposition (PECVD) system on a large area ($1.1 \times 1.3\ m^2$) substrate. The PECVD chamber has a multi-hollow cathode and a single radio-frequency (13.56 MHz) feed-through. The modules have a p-i-n structure on the TCO (SnO_2:F or ZnO:B) glasses. The thicknesses of the absorbing layers are 90–100 nm for the top cell (a-Si:H), 125–165 nm for the middle cell (a-SiGe:H), and 2.5–4.0 μm for the bottom cell (μc-Si:H). An n-μc-SiO_x:H intermediate layer was applied between the middle (a-SiGe:H) and bottom (μc-Si:H) absorbing layers. The H_2/SiH_4 gas ratio of the PECVD system are 8–10 for the top cell (a-Si:H), 50–70 for the middle cell (a-SiGe:H), and 60–90 for the bottom cell (μc-Si:H). The GeH_4/SiH_4 gas ratio is 0.08–0.1 for the middle cell.

The ZnO:B films as the TCO and BR layers were prepared by using the low pressure chemical vapor deposition (LPCVD) technique. Diethylzinc (DEZ) and water (H_2O) vapor were used as precursor gasses and directly evaporated in the system. Diborane (B_2H_6) was used as the doping gas (0.5% diluted in H_2). The ZnO:B films were deposited at a temperature between 180 and 190 °C. The thickness and doping gas ratio ($R = B_2H_6/DEZ$) of the ZnO:B films were varied by controlling the deposition time between 480 and 1440 s and the B_2H_6 gas flow between 300 and 1800 sccm. For BRs, white polyvinyl butyral was laminated on the ZnO:B in order to improve the light reflection from the rear side of the modules.

Measurements of the total and diffused optical transmittance (TT and DT, respectively) and total reflectance (TR) of the ZnO:B films on glass were carried out on a UV–vis spectrophotometer (JASCO V-670) equipped with an integrating sphere. The haze (DT/TT) was deduced from these measurements. Index matching liquid diiodomethane (CH_2I_2) was used to avoid the influence of roughness. The thickness was measured by a spectroscopic ellipsometer (Dainippon screen mfg RE-8000). The resistivity of the ZnO:B films was determined by a four-point probe measurement. The carrier concentration was evaluated by the Hall measurement.

The current voltage characteristics of the solar modules were measured under a solar simulator (Nishinbo PVS1222i-L) in standard test conditions (25 °C, AM 1.5 spectrum, 100 mW/cm^2). The external quantum efficiency (EQE) of each absorbing layer was measured from a 1 cm^2 electrode sampled from the large area cell.

3. RESULTS AND DISCUSSION

3.1. Smoothing effect of ZnO:B transparent conducting oxide with high haze

The performance of a superstrate type Si thin-film solar module strongly depends on the quality of the textured TCO glass substrate used for the front electrode. To improve the module power output, it is necessary to prepare a TCO glass substrate with a high transparency in the solar spectrum and to optimize the surface morphology for light scattering and the prevention of crack formations in the cell structure by controlling the deposition and texturing condition. In particular, it is well known that the crystal growth of μc-Si:H on ZnO grown by LPCVD gives rise to crack formation due to the rough surface morphology of ZnO, resulting in a reduction of the fill factor (*FF*) [14]. To solve this issue, Prof. Wenas *et al.*

have reported the surface smoothing process of boron-doped ZnO (ZnO:B) thin film by a two-step chemical vapor deposition (CVD) process using the DEZ/H_2O/ethanol reactant system, however, they did not fabricate the solar cell or module [15]. In our work, we first report the result of large area ($1.1 \times 1.3\ m^2$) Si thin-film solar modules using ZnO:B TCO glass substrate with smooth surface morphology using the DEZ/H_2O/ethanol reactant system.

ZnO:B films of approximately 1200 nm thickness were deposited on the $1.1 \times 1.3\ m^2$, 3.2 mm thick low iron glass substrate by the LPCVD process. A reference ZnO:B film was prepared by DEZ and H_2O as a precursor, and directly evaporated into the system. Diborane (B_2H_6) was used as the doping gas (0.5% diluted in H_2). The total pressure was kept at 0.3 Torr and the substrate was heated during ZnO:B film deposition at a temperature of 180 °C. On the other side, the ZnO:B film with a smooth surface morphology was prepared by two-step deposition. For the first step, a ZnO:B film was deposited under the same conditions as the reference ZnO:B film, then the DEZ/H_2O/ethanol reactant system was applied to prepare the smooth surface morphology of the ZnO:B film on the top of this deposited ZnO:B film. In order to study the effect of the change in the surface roughness, the process time of the second step was varied between 20 and 60 s in the DEZ/H_2O/ethanol reactant system. To evaluate the effect of the smooth surface morphology, the Si thin-film solar cells were on the reference and the smoothed surface of the ZnO:B TCO glass substrate.

Scanning electron microscope images and AFM topographies of the reference and smooth surface morphology of ZnO:B films prepared by the DEZ/H_2O/ethanol reactant system for 20, 40, and 60 s are shown in Figure 1. It is shown that the border line of the polycrystalline ZnO:B film became ambiguous as increasing the process time of DEZ/H_2O/ethanol reactant system, so the rough surface morphology of ZnO:B has become slightly smoother. Additionally, the surface roughness decreased in series, 52.4 nm (reference), 48.9 nm (20 s), 48.2 nm (40 s), and 47.9 nm (60 s) as increasing process time of DEZ/H_2O/ethanol reactant system. It is expected that the surface roughness would decrease and surface morphology would become smoother with the DEZ/H_2O/ethanol reactant process time. This smooth surface morphology results from the change of the dominant growth plane depending on the precursor combination. In the case of the DEZ/H_2O reactant system, the (110) plane is the dominant growth plane, while (002) and (001) are the dominant planes for the ZnO:B film prepared by the DEZ/H_2O/ethanol reactant system [15]. This smooth surface morphology of the ZnO:B substrate has potential for improving the *FF* of Si thin-film solar cells.

Figure 2 compares the optical properties of the reference ZnO:B substrate and the smooth morphology of ZnO:B substrates prepared by the DEZ/H_2O/ethanol reactant system. The transmittance of the reference and the smooth surface morphology of the ZnO:B substrates are almost the same for all the solar spectrum wavelengths. However, the haze ratio of the smooth surface morphology of the ZnO:B substrates is slightly lower than that of the reference ZnO:B. Especially, the haze ratio at wavelengths from 350 to 700 nm decrease as increasing process time of DEZ/H_2O/ethanol reactant system, which is caused by the decreased surface roughness.

Figure 3 presents the *I–V* results of a triple junction Si thin-film solar cell prepared on the reference and the smooth morphology of the ZnO:B glass substrate. The *FF* increases dramatically, on the other hand, the open-circuit voltage (V_{oc}) is almost same and the short-circuit current density (I_{sc}) slightly decreases as the DEZ/H_2O/ethanol reactant process time is over 40 s. The highest cell efficiency of 11.36% was obtained on the smooth surface morphology of the ZnO:B substrate prepared by using the DEZ/H_2O/ethanol reactant system for 40 s. In the case of the smooth surface morphology ZnO:B glass substrate with a process time of 60 s, the cell efficiency is lower than that with a time of 40 s, which results from the decrease of I_{sc}. Each cell (top/middle/bottom) has almost equivalent I_{sc} of 7.8 mA/cm^2, measured by Quantum efficiency. It seems that the I_{sc} loss of triple junction cell originates from I_{sc} loss of top cell, caused by the reduction of the haze ratio in 350–700 nm wavelength as shown in Figure 2.

Figure 4 shows the cross sectional image of triple junction Si thin-film solar cell prepared on the reference of ZnO:B substrate using transmittance electron microscopy. As shown in Figure 4, some micro-cracks have generated and penestrated from the surface of reference ZnO:B substrate into each layer of Si thin-film cell. It seems that the poor *FF* characteristic of triple junction Si thin-film cell prepared on the reference of ZnO:B substrate is originated from micro-cracks in the cell structure. Unfortunately, we could not have the comparison between the reference and the smooth surface morphology of ZnO:B substrate because it is difficult to measure the crack density quantitatively. We guessed that the crack density in the solar cells deposited on the smooth surface morphology of ZnO:B substrate could be reduced in comparison to that using the reference ZnO:B substrate. Improved cell efficiency (high *FF*) of the smooth morphology of ZnO:B can be considered by the lower crack density in the cell structure.

These results show that the surface smoothing process of the ZnO:B substrate using the DEZ/H_2O/ethanol reactant system is a very effective method to improve the performance of the Si thin-film module. Hereafter, all single and triple junction solar modules in this study were prepared on the smooth morphology of the ZnO:B substrate.

3.2. Window layer of multiphase silicon-carbon with low absorption loss

The interface between the front TCO and the top (a-Si:H) cell plays an important role in enhancing the photovoltaic properties of the Si thin-film solar cell. Although TCO, which is used in thin-film solar cells, exhibits good light transmittance and low resistivity, the work function difference between the TCO and the p-layer causes band

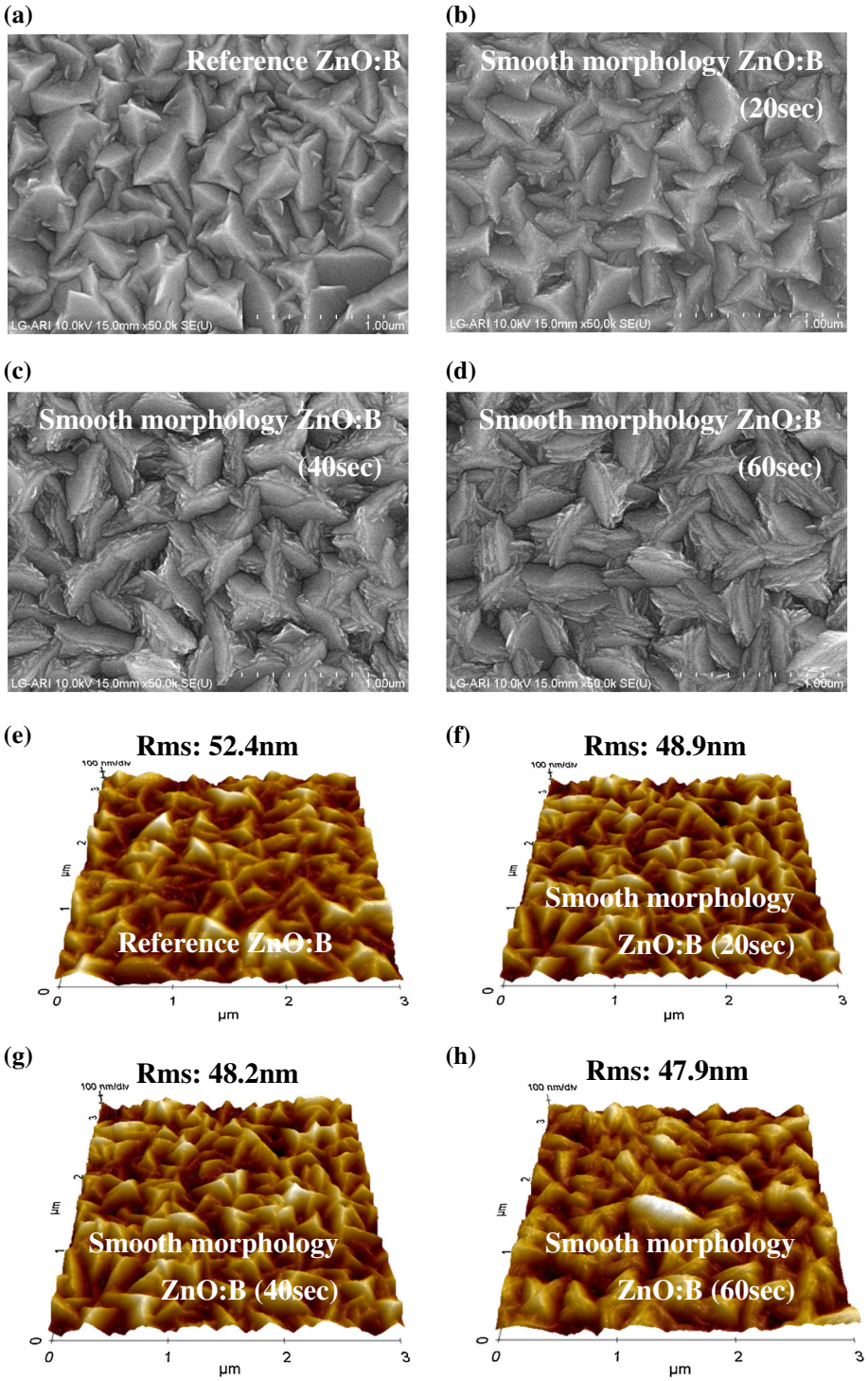

Figure 1. Surface morphology of ZnO:B substrate; (a) scanning electron microscope image of the reference ZnO:B, (b)–(d) scanning electron microscope image of the smoothed ZnO:B, (e) AFM image of the reference ZnO:B, and (f)–(h) AFM image of the smoothed ZnO:B.

bending and builds a potential barrier, which results in an imperfect ohmic contact [16]. This energy barrier can be reduced by the insertion of a highly conductive window layer, because it enables carriers to perform tunneling transport at the interface. Therefore, this layer is required to possess not only the property of low absorption in order to decrease the optical loss of incident light but also high conductivity to decrease the contact resistance.

DOI: 10.1002/pip

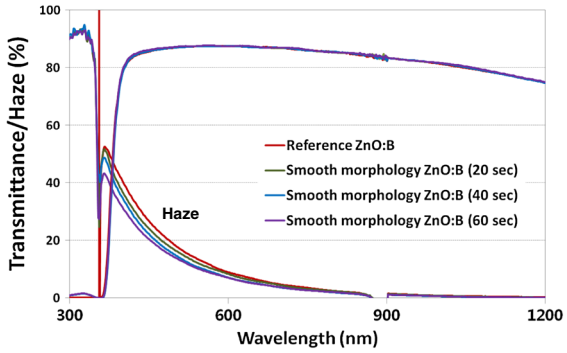

Figure 2. Optical transmittance spectra and haze ratios of reference and smooth surface morphology of ZnO:B substrates prepared by diethylzinc/H_2O/ethanol reactant system.

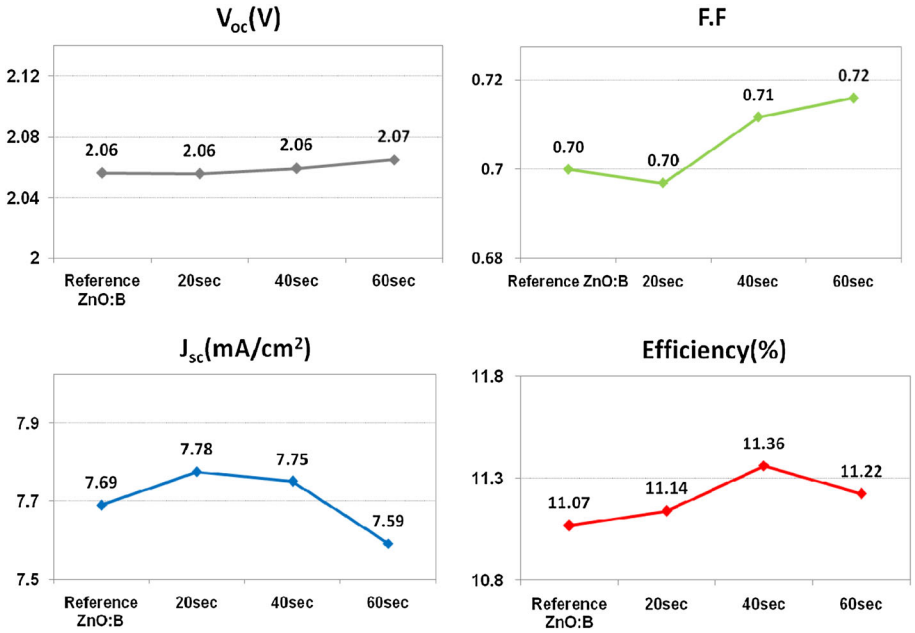

Figure 3. The results of triple junction Si thin-film solar cell on reference and smooth morphology of ZnO:B substrates prepared by different diethylzinc/H_2O/ethanol reactant process time.

The boron-doped microcrystalline silicon (p-μc-Si:H) has generally been used as the window layer in order to reduce the barrier [17,18]. An n-type microcrystalline silicon [19] and Ge [20] were also applied to solve the problem of the contact barrier. But these layers have serious optical losses at the short wavelength range. Even if boron-doped microcrystalline silicon carbide (p-μc-SiC:H) shows high transmittance and conductivity characteristics [21], it is inappropriate for mass production. This is because the p-μc-SiC:H has usually been deposited using electron-cyclotron resonance CVD, hot wire CVD, photo-CVD, etc. With these, it is very hard to control the uniformity of the large area module. The microcrystalline silicon oxide (μc-SiO:H) is very good candidate as window layer [22]. However, it has lower conductivity than p-μc-Si:H in our work. So far, it is consequently hard to improve the efficiency of cell. We are developing its deposition condition with superior conductivity.

To solve the aforementioned disadvantages, we suggest the application of the boron-doped hydrogenated multiphase silicon-carbon material, consisting of hydrogenated amorphous silicon (a-Si:H), hydrogenated amorphous carbon (a-C:H), and hydrogenated microcrystalline (μc-Si:H) phase as the window layer.

Figure 5(a) is the schematic atomic bond diagram of the multiphase silicon-carbon film proposed in this paper. It is represented with hydrogen, carbon, and silicon atoms, except for a few boron atoms. The carbon atoms mainly form an a-C:H phase of C–C bonds with a limited few Si–C bonds, and the silicon atoms grow into two phases of a-Si:H and μc-Si:H, as shown in Figure 5 (a). The a-C:H is more suitable for high transmission than amorphous silicon carbide (a-SiC:H) in the region of short wavelengths [23]. The formation of the μc-Si:H phase is favorable for obtaining a high level of conductivity.

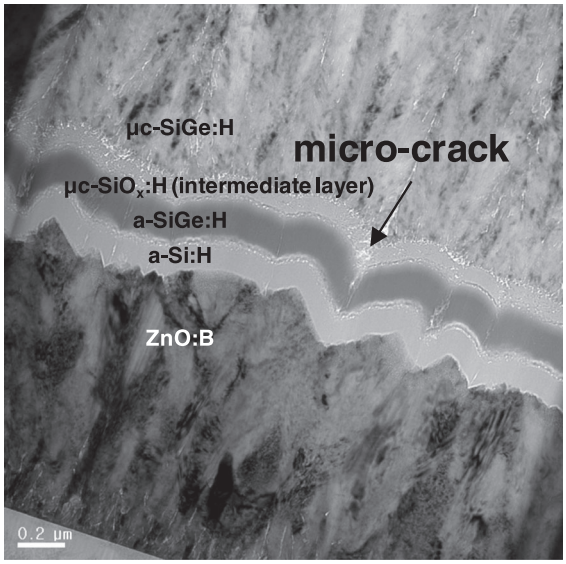

Figure 4. Transmittance electron microscopy image of micro crack in cell on reference ZnO:B substrate.

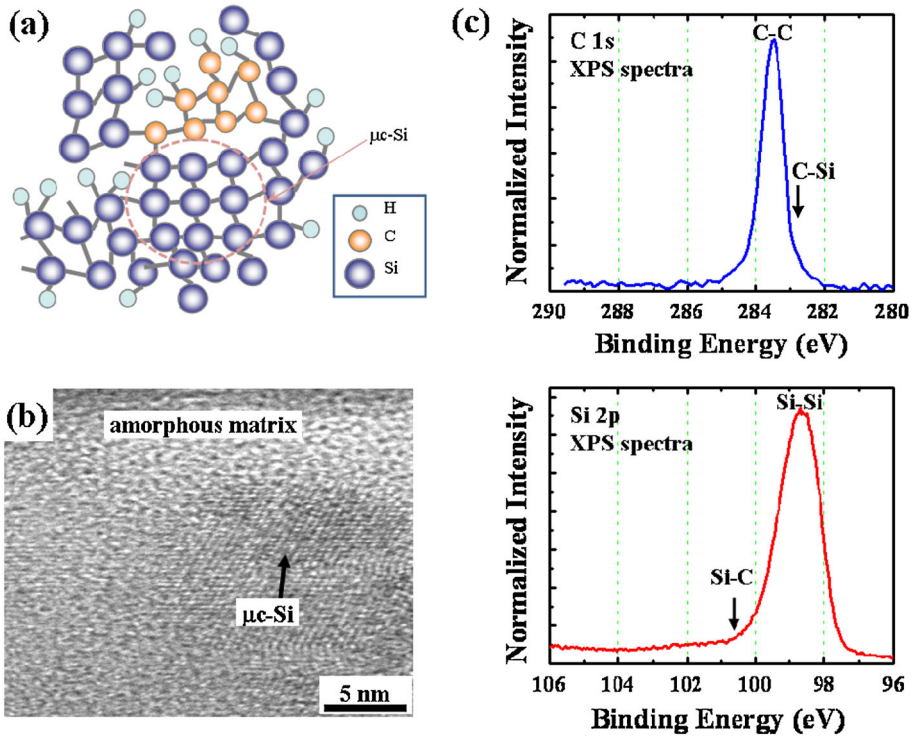

Figure 5. Atomic bond and microstructure analysis of multiphase silicon-carbon film: (a) schematic diagram of atomic bond, (b) cross-section image of high-resolution transmittance electron microscopy, and (c) X-ray photoelectron spectroscopy narrow scan of C 1 s (up) and Si 2p (down) [24].

The multiphase silicon-carbon film with 40 nm thickness grown on soda-lime glass was investigated by high-resolution transmittance electron microscopy and X-ray photoelectron spectroscopy (XPS) method. Figure 5(b) shows that the μc-Si:H precipitates dispersed in an amorphous matrix, such as a-C:H and a-Si:H. In order to investigate the chemical bonds of the amorphous matrix in the multiphase silicon-carbon film, the XPS narrow scan spectra were analyzed by Gaussian-Lorentzian curve fitting. Figure 5(c) shows the C 1 s and Si 2p peaks of the

XPS narrow scan spectra. The peak of the C–C bond has a very high intensity but the peak of the Si–C bond was rarely observed in the C 1 s peak (up). Similarly, the Si–C peak has a low intensity, and the Si–Si bond was mainly observed in the Si 2p peak (down). Therefore, it is confirmed that the multiphase silicon-carbon film consists of a-C:H, a-Si;H, and μc-Si:H, as shown in the schematic diagram as we suggested.

As shown in Figure 6(a), the optical absorbance of multiphase silicon-carbon is less than that of a conventional window layer (p-μc-Si:H) in the short wavelength range. The thickness of these films is 40 nm. Furthermore, multiphase silicon-carbon has a high conductivity of 2.5×10^{-2} S/cm, which was similar to that of p-μc-Si:H film. As a result, multiphase silicon-carbon film seems to be a superior candidate for the front contact layer in Si thin-film solar cells.

Figure 6(b) shows the EQE of a-Si/a-SiGe double junction solar cells with a 5 nm thick window layer. The solar cell with a multiphase silicon-carbon layer showed a higher EQE in the short wavelength region, as expected. The conversion efficiency is 10.8%, which is higher by about 0.6% than the solar cell with the p-μc-Si:H layer. This result is due to the low optical loss of the multiphase silicon-carbon layer, resulting in a current density (I_{sc}) increase in the a-Si:H layer.

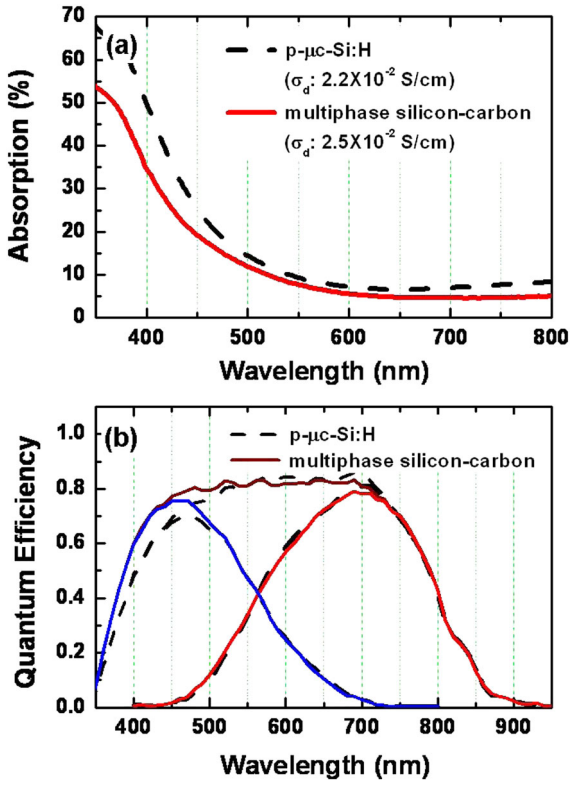

Figure 6. (a) Optical absorbance calculated from measured transmittance and reflectance in films with 40 nm thickness according to the wavelength and (b) external quantum efficiency according to the window layer [24].

In summary, the multiphase silicon-carbon film has the good properties of a little optical absorption loss at short wavelengths and high electrical conductivity. We verified that it is very effective when it is applied as a window layer in Si thin-film solar cells. This section was written minutely in our previous publication [24].

3.3. Intermediate layer with low refractive index

In the multi-junction Si thin-film solar cells, the amorphous absorbing layers should be thin to minimize the light-induced degradation effect, which can reduce the device current by the reduced current of the amorphous absorbing layers. An intermediate layer is introduced to increase the current of the amorphous absorbing layers without increasing their thicknesses [9]. In the case of the triple junction (a-Si:H/a-SiGe:H/μc-Si:H) cell, the intermediate layer can be adapted between the middle (a-SiGe:H) and the bottom (μc-Si:H) cells [7]. Among the materials of intermediate layer, n-μc-SiO_x:H is one of the promising materials due to its lower refractive index and lower absorption of light in the longer wavelength region, compared with the ZnO-based intermediate layers [25,26].

The high quality of the intermediate layer should reflect more light due to the lower refractive index, which usually leads to a lower electric conductivity. The intermediate layer with an electric conductivity lower than a certain level cannot function well in the solar cell due to its poor contact performance, leading to a high series resistance (R_s) and a low *FF*. In general, it is known that the vertical electrical conductivity has to be $>1E^{-5}$ S/cm to function well in the solar cell [27]. However, it is not easy to measure the electrical conductivity vertically. Therefore, many groups used co-planar or Raman spectroscopy to analogize the vertical conductivity [4,7,9,25]. We solved this problem by analyzing the conductive atomic force measurement (C-AFM) [7]. As shown in Figure 7, four n-μc-SiO_x:H intermediate layers with different refractive indices are analyzed by C-AFM. In this analysis, a 1.5 V bias voltage is applied to the $5 \times 5\ \mu m^2$ area. Dark spots indicate a higher current flowing at those spots. The intermediate layers are ~100 nm thick. Dark areas are rare in Figure 7(a). Light gray spots are distributed in (b). In (c) and (d), dark gray spots are distributed in the overall area. The sample A has a refractive index (n) as low as 1.67, and the average current measured by C-AFM is similar to the noise level. Sample B ($n = 1.73$) has a 50 times higher than average current compared with sample A, which shows that sample B has a vertically conductive area. Samples C and D have higher average currents than sample B, indicating that they are more vertically conductive than sample B. From the preceding text, we expect that samples B, C, and D have vertical conductivities favorable enough to apply in the solar cell. Sample B is expected to have the best reflection property among the samples due to the lowest refractive index.

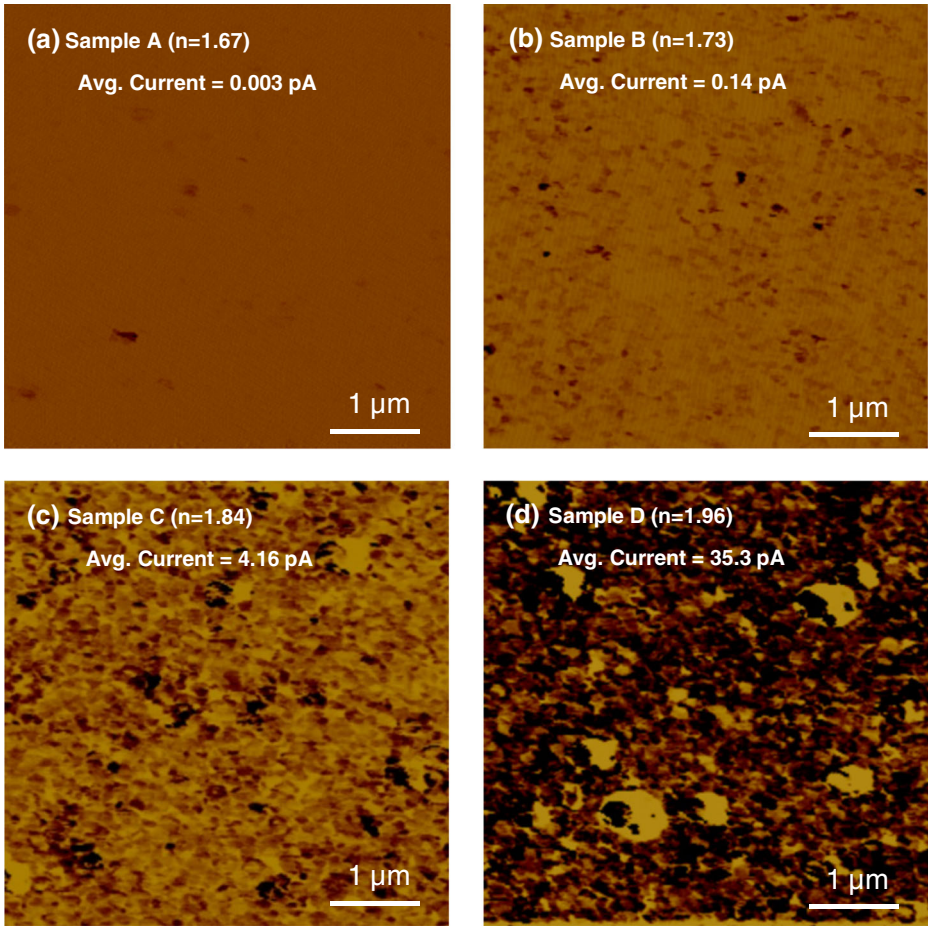

Figure 7. Current images of the n-μc-SiO_x:H thin films analyzed by conductive atomic force microscopy. (a) refractive index [*n*] = 1.67, (b) *n* = 1.73, (c) *n* = 1.84, and (d) *n* = 1.96 [10].

Three intermediate layers (samples B, C, and D) are applied in the triple junction solar cell between the middle (a-SiGe:H) and bottom (μc-Si:H) cells with a thickness of 75 nm. Figure 8 shows the EQE of each absorbing layer of the solar cells as a function of the refractive index of the intermediate layer. The middle cell current (a-SiGe:H) increases in the 600–800 nm range as the refractive index of the intermediate layer decreases. This means the intermediate layers, which have a lower refractive index, can reflect the light in that range effectively, which can maintain the current density of the middle cell with a thinner a-SiGe:H layer. A thinner a-SiGe:H layer is expected to increase the V_{oc} and *FF* in the module.

Table I shows the initial properties of the large area module as a function of the refractive index of the intermediate layer and the thickness of the a-SiGe:H absorbing layer. There was no loss of I_{sc} of sample B due to its lower refractive index compared with those of samples C and D, even though sample B is thinner than sample D by 20 nm and than sample C by 10 nm. In addition, sample B has higher V_{oc} and *FF* than other samples due to its thinner a-SiGe:H absorbing layer, which is more defective than the other absorbing layers. As a result, the initial conversion efficiency of sample B is 12.02%, which is ~0.3% higher than sample D and ~0.1% higher than sample C. On

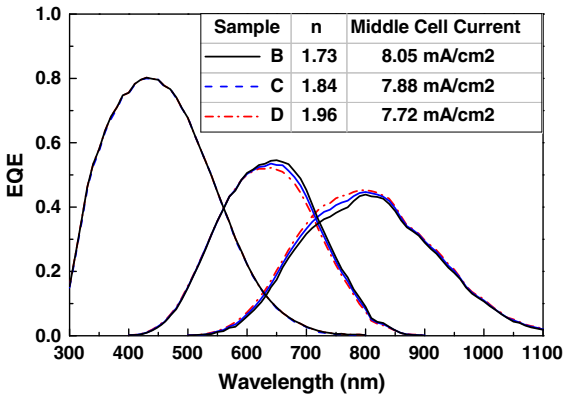

Figure 8. External quantum efficiency (EQE) of 1 cm^2 size triple junction cells prepared with different refractive indices (*n*) of the n-μc-SiO_x:H intermediate layer. The inlet table indicates the middle cell current of each sample [10].

Table I. The initial conversion efficiencies and some other properties of the large area ($1.1 \times 1.3\,m^2$) modules as a function of the refractive index of the intermediate layer and the thickness of the a-SiGe:H layer.

Sample (IL)	Refractive index of IL	Thickness of a-SiGe:H layer (nm)	V_{oc} (V)	I_{sc} (A)	Fill factor	Efficiency (%)
A	1.67	135	224.6	0.572	0.423	3.94
B	1.73	145	230.1	0.990	0.726	12.02
C	1.84	155	229.7	0.990	0.723	11.94
D	1.96	165	228.5	0.989	0.715	11.74

IL, intermediate layer.

the other hand, sample A has poor *FF* and efficiency because its intermediate layer does not have sufficient conductivity, which increases drastically the resistance of the device, as expected. This section was written fully in our previous publication [10].

3.4. Hydrogenated microcrystalline silicon layer with uniform thickness and crystalline volume fraction

μc-Si:H has been a widely used material for thin-film solar cells. In particular, because μc-Si:H has a bandgap of 1.1 eV, it could be used as a bottom cell in a-Si:H/μc-Si:H tandem solar cells or a-Si:H/a-SiGe:H/μc-Si:H triple junction solar cells. In the multi-junction solar cells, the μc-Si:H layer also plays a significant role in providing a high conversion efficiency and high stability as an absorber material for the long wavelength region near the infrared [28,29]. In large area multi-junction thin-film solar cells, the uniformity of the μc-Si:H layer, such as regarding its thickness and crystalline volume fraction, is very important to enhance the photovoltaic properties of silicon thin-film solar cells, due to the fact that the lowest property restricts the conversion efficiency in a large area solar cell module. In order to improve the lateral and vertical distribution of the μc-Si:H layer, we have investigated the design of the showerhead in PECVD and the profile scheme of the H_2/SiH_4 ratio during the film deposition, respectively.

All the μc-Si:H layers were prepared by radio-frequency PECVD using a gas mixture of SiH_4 and H_2. The thickness of the μc-Si:H solar cells was maintained at 3.0 μm, and they were deposited in a p-i-n structure on the TCO (SnO_2:F or ZnO:B) substrate with a large area ($1.1 \times 1.3\,m^2$) size. The structural properties of the films were investigated by spectroscopic ellipsometry and Raman spectroscopy measurements with 25 point measurements in a large area. To measure the crystalline volume fraction of μc-Si:H, Raman spectroscopy with a wavelength of 532 nm was used. The crystalline volume fraction was defined as the ratio of the integrated area of the μc-Si:H peak at $520\,cm^{-1}$ (I_{520}) to the total peak area ($I_{520} + I_{510} + I_{480}$). The non-uniformity (%) was obtained by using the following formula, (Max-Min)/(Max + Min) × 100, where Max and Min were the maximum and minimum values of the measurements.

Figure 9 shows the non-uniformity of thickness and the crystalline volume fraction (X_c) in μc-Si:H layer prepared with two different multi-hollow cathode showerhead type, where S/H-1 and S/H-2 refer to the conventional and our modified showerhead, respectively. In the case of S/H-1 (conventional showerhead), the thickness non-uniformity of μc-Si:H layer is 11% and X_c is 5.0% in $1.1 \times 1.3\,m^2$, as shown in Figure 9(a) and (b). There is the tendency that values of thickness and X_c increase toward center area. In order to reduce the non-uniformity of film, the showerhead was modified to the concave shape cathode, and the gas dispersion system was added in it. Applying the S/H-2 (modified showerhead), we obtained the superior uniformity of μc-Si:H layer that the thickness and X_c non-uniformities were reduced from 11% to 4.1% and from 5.0% to 2.0%, respectively, as shown in Figure 9(c) and (d).

Next, to obtain the uniform crystalline volume fraction in the thickness direction of μc-Si:H layer, we controlled the H_2/SiH_4 gasses ratio in the early stage of deposition. It is well known that μc-Si:H grows from an amorphous phase to a crystal phase at the initial stage of film deposition and that the crystalline volume fraction increases as the film thickness increases. Figure 10(a) shows the profiling scheme of the H_2/SiH_4 gasses ratio. The line represents a constant H_2/SiH_4 ratio during the deposition, and the dot line illustrates the profile scheme with a high H_2/SiH_4 gasses ratio in the initial stage, and the H_2/SiH_4 ratio gradually decreases to the middle stage. Figure 10(b) demonstrates the crystalline volume fraction results of each profiling scheme. The samples are prepared with certain thicknesses and measured using Raman spectroscopy in a large area ($1.1 \times 1.3\,m^2$). The case of a constant H_2/SiH_4 ratio shows a low crystalline volume fraction of 45% in the initial stage and that it saturates after the middle stage. In contrast, a high H_2/SiH_4 ratio in the initial stage shows that there is almost a constant crystalline volume fraction as a function of the film thickness. This means that the structural properties are the same regardless of the film thickness.

In summary, our modified showerhead and profiling schemes are successfully applied in the μc-Si:H layer, which result in a good uniform distribution of thickness and crystalline volume fraction in the lateral and vertical directions. It is expected to result in a high efficiency solar module using this absorber layer as the bottom in the triple junction thin-film solar cell.

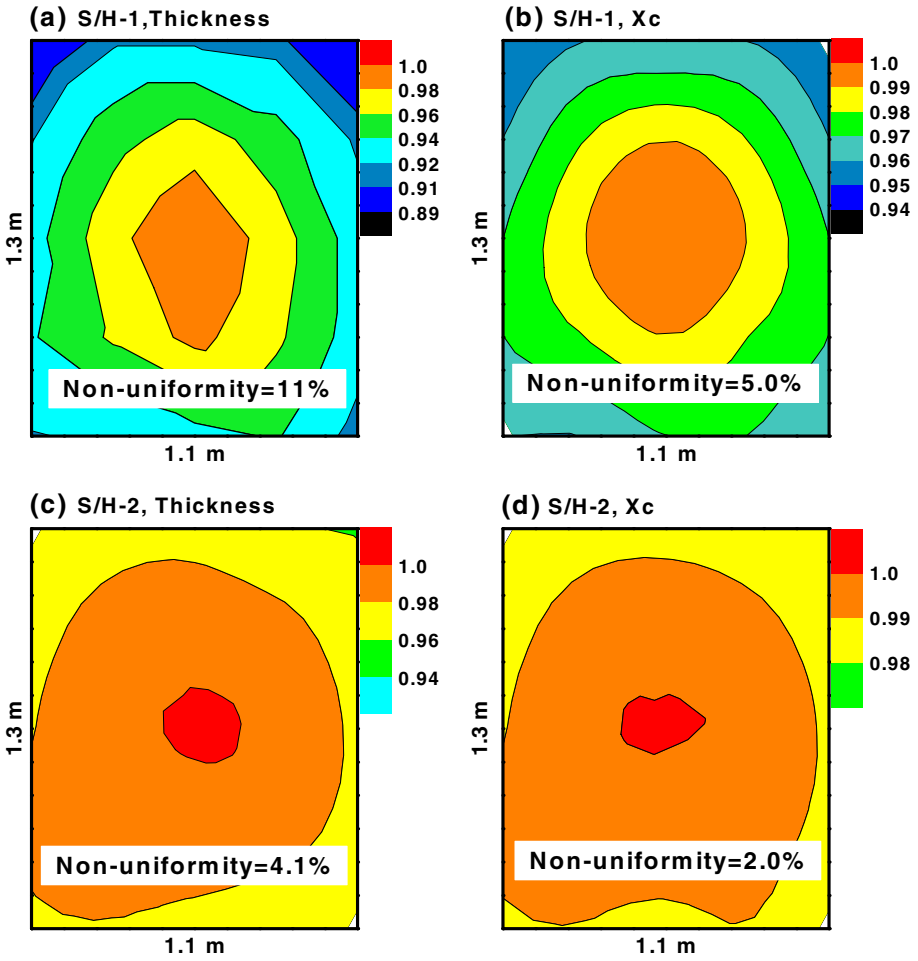

Figure 9. Non-uniformity of thickness and the crystalline volume fraction (X_c) in μc-Si:H layer prepared with two different multi-hollow cathode showerhead type. S/H-1 is conventional and S/H-2 is our modified showerhead. (a) thickness distribution in S/H-1 case, (b) X_c distribution S/H-1 case, (c) thickness distribution in S/H-2 case, and (d) X_c distribution in S/H-2 case.

3.5. Boron-doped zinc oxide BR with high haze and low absorption

A BR is used to enhance the light trapping, specifically by reflecting long wavelength light into the bottom cell. A BR should show a high haze and a high reflection for scattering and reflecting the light at the back [30]. Some TCOs, which demonstrate light scattering and high conductivity properties at once, are used as a BR as well as a back electrode simultaneously because they could substitute metal back electrode [31]. The sputter grown and wet-etched aluminum-doped zinc oxide (ZnO:Al) shows the highest haze among typical TCOs, however, its utilization as BR to mass production is limited. The sputter grown ZnO:Al with smooth surface morphology requires wet-etch process, which is not applicable in the BR production process in a superstrate (*p-i-n*) configuration [32]. The boron-doped zinc oxide (ZnO:B) also demonstrates high haze due to a naturally grown rough surface morphology and is suitable for a superstrate (*p-i-n*) configuration [33]. This simple production process enables ZnO:B to be a good candidate for a BR. We have implemented the ZnO:B as a back electrode as well as a BR.

It is known that the haze of the ZnO:B BR is influenced by the thickness: the thicker the ZnO:B BR, the higher the haze [33]. We also have applied the ZnO:B BR with the thickness into the solar modules. As shown in Table II, as the thickness of the ZnO:B BR increases, the maximum power output (P_{max}) slightly increases due to the combination of a decreased I_{sc} and an increased *FF*. The light trapping by the thick BR is not effective as we expected. We noticed there was another main factor as well as the haze due to the thickness of ZnO:B BR. We expect that the other factor was the absorption of ZnO:B BR.

In this paper, we have focused on the development of the ZnO:B BR with low absorption to improve the I_{sc} of the solar modules and to reduce the i-μc-Si thickness. The doping gas ratio (B_2H_6/DEZ) of the BR was controlled in order to meet the objective.

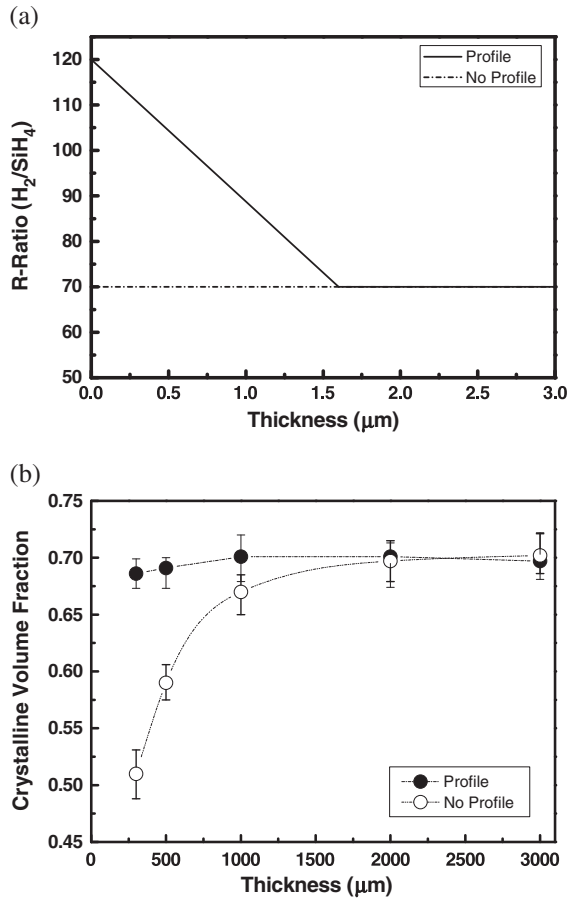

Figure 10. (a) The profiling scheme of H_2/SiH_4 gasses ratio as a function of layer thickness. (b) The crystalline volume fraction results of each profiling scheme as a function of layer thickness.

Table II. The *I–V* parameters of the large area ($1.1 \times 1.3\,m^2$) triple junction Si thin-film solar modules as a function of the ZnO:B BR thickness.

Thickness of ZnO: B BR (μm)	V_{oc} (V)	I_{sc} (A)	Fill factor	P_{max} (W)
1.0	228.2	1.005	0.696	159.6
2.1	228.2	1.002	0.699	160.0
2.7	228.7	1.001	0.703	161.0

First, we have deposited the ZnO:B films with the doping gas ratios (B_2H_6/DEZ) directly on a glass substrate to evaluate the haze and the absorption. Figure 11 shows the haze and the absorption spectra, equal to 1-TT-TR, as a function of the doping gas ratio of the ZnO:B film. As the doping gas ratio decreases, the haze slightly increases because the surface roughness increases due to the enlarged ZnO:B grain [34]. The absorption of the film decreases because the free carrier absorption by the dopants in the ZnO:B film proportionally decreases [35]. In short, the lower doping gas ratio of the ZnO:B film demonstrates both the higher haze and the lower absorption simultaneously.

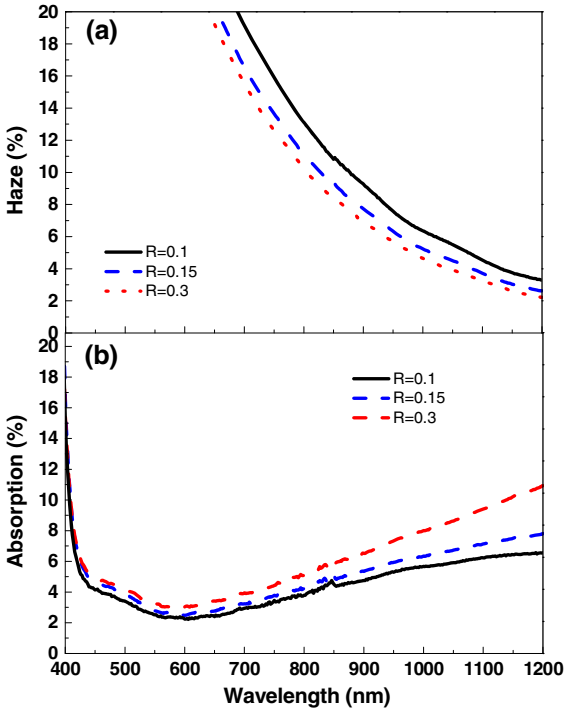

Figure 11. (a) The haze and (b) absorption spectra of the ZnO:B films with different doping gas ratios (B_2H_6/diethylzinc) [31].

Second, these ZnO:B BRs were applied into the solar modules. Figure 12 presents the *I–V* results of the large area ($1.1 \times 1.3\,m^2$) triple junction (a-Si:H/a-SiGe:H/μc-Si:H) Si thin-film solar modules with doping gas ratios as a function of the i-μc-Si film thickness. The solar modules were fabricated to investigate the influence of the absorption of the ZnO:B BR on the solar module parameters. It is considered that the absorption of the BR strongly influences the bottom cell performance, especially the i-μc-Si layer thickness.

As the i-μc-Si thickness decreases, P_{max} and I_{sc} gradually decrease, while V_{oc} and *FF* are independent over all doping gas ratios. As thinner i-μc-Si thickness, there is less chance to absorb the light at the i-μc-Si layer, which results in a decrease in I_{sc}. As clearly shown in Figure 12, the I_{sc} is the main factor contributing to the P_{max} as we predicted. For an i-μc-Si thickness of 3 μm, P_{max} increases by about 2.5 W by lowering the doping gas ratio from 0.3 to 0.1. This means that the ZnO:B BR with the lower doping gas ratio brings better light trapping properties into the i-μc-Si layer due to the lower absorption of the BR, which therefore improves I_{sc}.

We could also reduce the i-μc-Si layer thickness from ~3.25 to ~2.35 μm for an equivalent I_{sc} by reducing the doping gas ratio from 0.3 to 0.1. It is clearly seen that the ZnO:B BR with the lower doping gas ratio is also effective at enabling a decrease in the thickness of the i-μc-Si layer. This reduces the i-μc-Si layer thickness by approximately ~28%, which provides a shorter i-μc-Si layer deposition time and a cheaper manufacturing cost. In short, a low

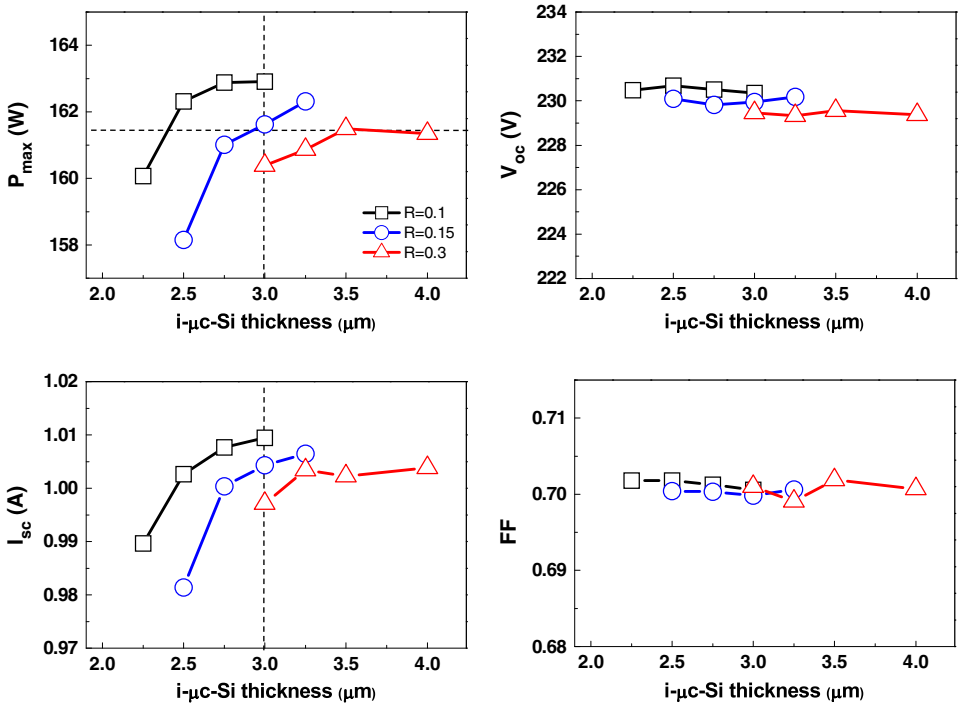

Figure 12. The *I–V* results of the triple junction Si thin-film solar modules with different ZnO:B back reflector doping gas ratios as a function of the i-μc-Si thickness [31].

doping gas ratio is favorable for increasing I_{sc} and decreasing the i-μc-Si layer thickness by improving the light trapping ability.

In this work, we noticed that the ZnO:B BR with the high haze and low absorption due to the lower doping gas ratio is found to be more effective in light trapping and in reducing the i-μc-Si layer thickness. We could reduce the i-μc-Si layer thickness by about ~30% with the low doping gas ratio for an equivalent P_{max} level and improve the P_{max} about 2.5 W for an equivalent i-μc-Si layer thickness. We successfully implemented the BR with high haze and low absorption into the triple junction Si thin-film solar. This related full article has been published [31].

3.6. Approach to optimize the performance of solar modules

3.6.1. Current matching method in large area solar modules.

In multi-junction solar cells, the current density of each component cell (top, middle, bottom) should be matched to maximize the current of the overall cell because the component cells are connected in series. However, in the large area module, there are additional issues regarding the current matching. First, the properties of each film are not so uniform in general, depending on the position in the large area module [36]. In particular, a difference in the thickness usually leads to a difference in the current. Second, the large area module consists of narrow rectangular cells fabricated by the laser scribing technique [37,38], as shown in Figure 13(a). The current of the large area module is the smallest value among the limiting component cell currents of each rectangular cell.

To measure the current of each component cell in a certain position in the module, we should make a small cell (~1 cm^2) at that position, called a "coupon cell". To measure the current in the whole area of the module precisely, we have to make numerous coupon cells all over the positions in the large area module, measure the EQE of each component cell of each coupon cell, and add the values in a cell, which is very laborious. We simplified the method of the current matching by collecting the EQE data of 25 (5 × 5) coupon cells in the large area module, as shown in Figure 13(a), which can be used as an index of the current matching in the large area module.

We obtained the current of each component cell of the 25 coupon cells in a large area module based on the EQE data, as shown in Figure 13(b)–(d). The top and middle cell currents are somewhat uniform with a difference of 0.2–0.3 mA/cm^2 in the module, the bottom cell current has a large difference of ~0.8 mA/cm^2. On the basis of this result, we calculated the average current of each component by averaging the five current densities. For cell A in Figure 13(a), the values are the average of the coupon cells #1–#5. Table III shows the result. The bottom cell current limits the current of the each cell except for cell C. In particular, the bottom cell current at the edge (cell A, cell E) limits the current of the whole module. In this case, we can increase the module current by increasing the bottom cell current at the edge.

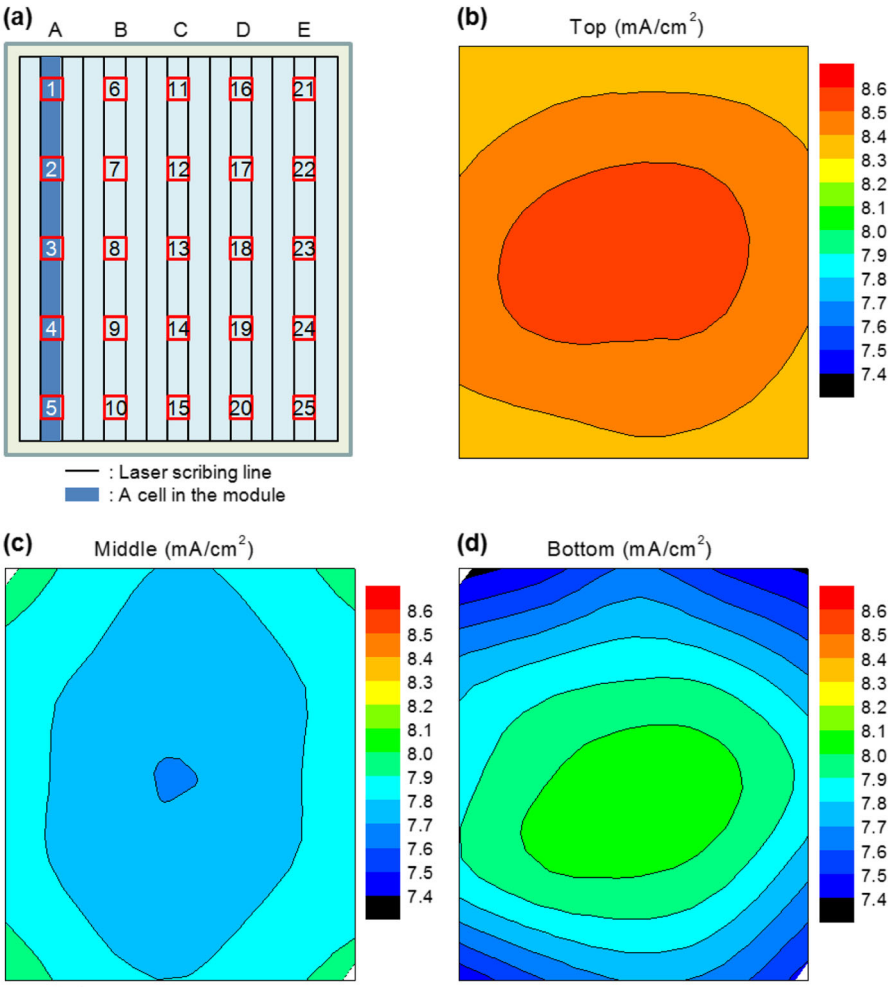

Figure 13. (a) The schematic structure of the large area module indicating the laser scribing lines and a cell defined by the scribing lines, the positions of the 25 coupon cells. (b)–(d) The contours of the current densities of the component cells (top, middle, bottom) as a function of the position in the module, on the basis of the external quantum efficiency data of the 25 coupon cells.

3.6.2. Stability improvement of the solar module under long-term light illumination.

In order to make a Si thin-film solar cell competitive with other technologies, it needs to minimize the light-induced degradation by the Staebler–Wronski effect as well as to improve the conversion efficiency. It is well known that meta-stable defect generation induced by prolonged illumination leads to degradation in hydrogenated amorphous silicon (a-Si:H)-based solar cells [39]. In a multi-junction cell, each component cell has to be taken into account in order to decrease the degradation rate. In particular, we have concentrated on reducing the thickness of the a-SiGe:H absorber layer, because the a-SiGe:H single cell generally shows faster degradation than the a-Si:H single cell [40].

In this paper, there are two approaches for the reduction of middle cell thickness. One is reducing the refractive index of interlayer to enhance the reflection toward the middle cell. The interlayer of n-μc-SiO:H with each refractive index of 1.75, 1.79, and 1.85 was used in the triple junction cells. The other approach is the increase of the front TCO haze to lengthen the effective optical path length. The haze of the TCO developed in this work increased the haze by up to 15% at a wavelength of 650 nm, which is mainly absorbed in the a-SiGe:H middle cell. These approaches are able to obtain more absorption of the light in the a-SiGe:H middle cell and reduce its thickness.

Figure 14 shows the degradation rate in the triple junction Si thin-film module as a function of the middle cell thickness. The stabilization of the modules was performed under the light-soaking conditions of IEC61646. The degradation rate of the modules decreased in proportion to the middle cell thickness and was reduced to 7.6%. It is a progressive result for large area Si thin-film solar modules using a triple junction structure.

3.6.3. Remarkable steps of Si thin-film solar modules at LG Electronics.

We have consistently developed the main items such as front TCO smoothing with high haze, a low absorption

Table III. The average current density of the component cells of each rectangular cell, based on the EQE data of the 25 coupon cells.

Cell	A	B	C	D	E
Top	8.38	8.43	8.45	8.43	8.36
Middle	7.88	7.80	7.78	7.80	7.89
Bottom	7.65	7.77	7.85	7.79	**7.62**

The underlined numbers indicate the limited component cell of each rectangular cells, the bold underlined number indicates the limited component cell of the whole module.

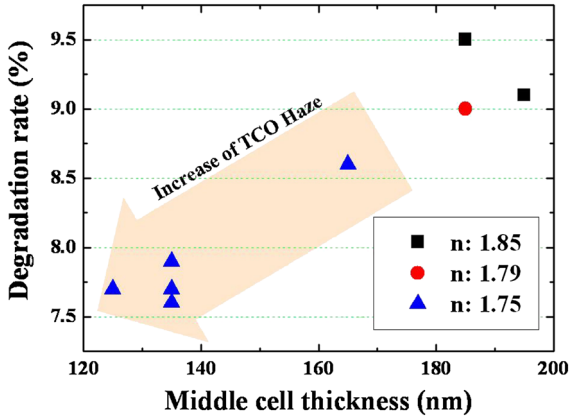

Figure 14. Degradation rate in triple junction Si thin-film solar cell as a function of the thickness of middle cell.

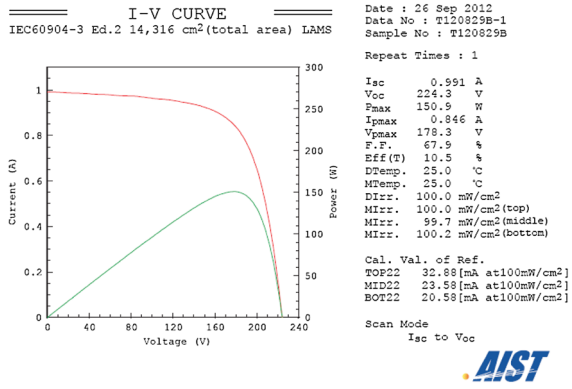

Figure 15. The photovoltaic performance of a-Si:H/a-SiGe:H/μc-Si:H thin-film solar module measured at Advanced Industrial Science and Technology.

window layer, interlayer with a low refractive index, uniformity control of the thickness and volume crystalline fraction in the microcrystalline silicon layer, and a BR with high haze and low absorption.

In particular, we achieved a stabilized output power of 151 W in a large area Si thin-film solar module, measured by own simulator. It was confirmed by AIST at the end of 2012, as shown in Figure 15. The stabilized output power of 151 W was obtained in this module. It was the efficiency of 10.5% (V_{oc} = 224.3 V, I_{sc} = 0.991 A, FF = 0.679) in total module area.

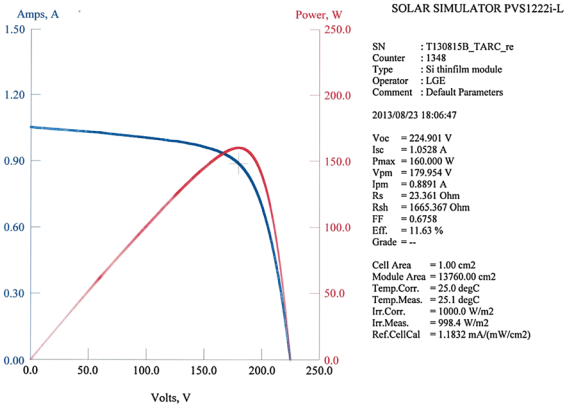

Figure 16. The photovoltaic performance of a-Si:H/a-SiGe:H/μc-Si:H thin-film solar module improved up to 160 W.

Recently, we have improved this record and increased the stabilized output power up to 160 W. Figure 16 shows the in-house measurement result of our best Si thin-film solar module. The stabilized efficiency improved up to 11.2% in the total module area. It was obtained by an increase of I_{sc} due to the enhancement of light trapping technology.

4. CONCLUSIONS

We have developed a large area (1.1 × 1.3 m^2) Si thin-film solar module with a triple junction cell (a-Si:H/a-SiGe:H/μc-Si:H) providing efficient light utilization. In particular, we have focused on light trapping technologies such as the smoothing of high haze TCO, a low absorption window layer, a low refractive index interlayer, uniformity control of the thickness and crystalline volume fraction in the microcrystalline silicon layer, and a low absorption BR. These features were successfully implemented into the triple junction Si thin-film solar module.

Through these works, we have achieved world records of a 13.4% stabilized efficiency in the small size (1 cm^2) and a 10.5% stabilized efficiency in the large area module (1.1 × 1.3 m^2), certificated by National Renewable Energy Laboratory and AIST, respectively. These results were presented in Solar cell efficiency tables (Version 41). At this moment, we have improved on these records and increased the result to a module output power of 160 W and a stabilized efficiency of 11.2% in the large area module (1.1 × 1.3 m^2), measured by our own solar simulator. We have verified and believe that focusing on light trapping technologies is most effective way to achieve a high efficiency solar cell.

REFERENCES

1. Heinstein P, Ballif C, Perret-Aebi LE. Building integrated photovoltaics (BIPV): review, potentials, barriers and myths. *Green* 2013; **3**: 125–156.

2. Jardine C, Conibeer G, Lane K. PV-COMPARE: direct comparison of eleven PV technologies at two locations in northern and southern Europe. *Proceedings of 17th European PVSEC* 2001.
3. van Cleef M, Lippens P, Call J. Superior energy yields of Uni-Solar triple junction thin film solar cells compared to crystalline Si solar cells under real outdoor conditions in Western Europe. *Proceedings of 17th European PVSEC* 2001.
4. Yang J, Banerjee A, Guha S. Triple-junction amorphous silicon alloy solar cell with 14.6% initial and 13.0% stable conversion efficiencies. *Applied Physics Letters* 1997; **70**: 2975–2977.
5. Deng X. Optimization of a-SiGe based triple, tandem and single-junction solar cells, *Conference Record of the 31st IEEE Photovoltaic Specialists Conference* 2005; 1365–1370.
6. Bailat J, Fesquet L, Orhan JB, Djeridane Y, Wolf B, Madliger P, Steinhauser J, Benagli S, Borrello D, Castens L, Monteduro G, Marmelo M, Dehbozorghi B, Vallat-Sauvain E, Multone X, Romang D, Boucher JF, Meier J, Kroll U, Despeisse M, Bugnon G, Ballif C, Marjanovic S, Kohnke G, Borrelli N, Koch K, Liu J, Modavis R, Thelen D, Vallon S, Zakharian A, Weidman D. Recent developments of high-efficiency micromorph tandem solar cells in KAI-M PECVD reactors, *Proceedings of the 25th European Photovoltaic Solar Energy Conference and the 5th World Conference on Photovoltaic Energy Conversion* 2010; 2069–2073.
7. Yan B, Yue G, Sivec L, Yang J, Guha S, Jiang CS. Innovative dual function nc-SiO_x:H layer leading to a >16% efficient multi-junction thin-film silicon solar cell. *Applied Physics Letters* 2011; **99**: 113512-1–113512-3.
8. Green M, Emery K, Hishikawa Y, Warta W, Dunlop ED. Solar cell efficiency tables (version 41). *Progress in Photovoltaics: Research and Applications* 2013; **21**: 1–11.
9. Fischer D, Dubail S, Selvan JAA, Vaucher NP, Platz R, Hof CH, Kroll U, Meier J, Tomes P, Keppner H, Wyrsch N, Goetz M, Shah A, Ufert KD. The "micromorph" solar cell: extending a-Si:H technology towards thin film crystalline silicon, *Conference Record of the 35th IEEE Photovoltaic Specialists Conference* 1996; 1053–1056.
10. Hwang ST, You DJ, Kim SH, Lee S, Lee HM. Large area Si thin film solar module applying n-μc-SiO_x:H intermediate layer with low refractive index. *Solar Energy Materials and Solar Cells* 2013; **113**: 79–84.
11. Beneking C, Rech B, Wieder S, Kluth O, Wagner H, Frammelsberger W, Geyer R, Lechner P, Rubel H, Schade H. Recent developments of silicon thin film solar cells on glass substrates. *Thin Solid Films* 1999; **351**: 241–246.
12. Kluth O, Rech B, Houben L, Wieder S, Schope G, Beneking C, Wagner H, Loeffl A, Schock H. Texture etched ZnO:Al coated glass substrates for silicon based thin film solar cells. *Thin Solid Films* 1999; **351**: 247–253.
13. Rech B, Repmann T, van den Donker MN, Berginski M, Kilper T, Hüpkes J, Calnan S, Stiebig H, Wieder S. Challenges in microcrystalline silicon based solar cell technology. *Thin Solid Films* 2006; **511–512**: 548–555.
14. Sakai H, Yoshida T, Hama T, Ichikawa Y. Effects of surface morphology of transparent electrode on the open-circuit voltage in a-Si:H solar cells. *Japanese Journal of Applied Physics* 1990; **29**: 630–635.
15. Wenas WW, Konagai M. Control of the surface morphology of ZnO thin films for solar cells by novel two-step MOCVD process, *Photovoltaic Specialists Conference Record of the 29th IEEE* 2002; 1130–1132.
16. Sinencio FS, Williams R. Barrier at interface between amorphous silicon and transparent conducting oxides and its influence on solar cell performance. *Journal of applied physics* 1983; **54**: 2757–2760.
17. Lee J, Dutta V, Yoo J, Yi J, Song J, Yoon KH. Superstrate p-i-n a-Si:H solar cells on textured ZnO: Al front transparent conduction oxide. *Superlattices and Microstructures* 2007; **42**: 369–374.
18. Schwanitz K, Klein S, Stolley T, Rohde M, Severin D, Trassl R. Anti-reflective microcrystalline silicon oxide p-layer for thin-film silicon solar cells on ZnO. *Solar Energy Materials and Solar Cells* 2012; **105**: 187–191.
19. Kubon M, Boehmer E, Siebke F, Rech B, Beneking C, Wagner H. Solution of the ZnO/p contact problem in a-Si:H solar cells. *Solar Energy Materials and Solar Cells* 1996; **41–42**: 485–492.
20. Kim J, Abou-Kandil AI, Hong AJ, Saad MM, Sadana DK, Chen TC. Efficiency enhancement of a-Si:H single junction solar cells by a-Ge:H incorporation at the p+ a-SiC:H/transparent conducting oxide interface. *Applied Physics Letters* 2011; **99**: 062102-1–062102-3.
21. Ma W, Aoyama S, Okamoto H, Hamakawa Y. A study of interface properties in a-Si solar cells with μc-Si(C). *Solar Energy Materials and Solar Cells* 1996; **41–42**: 453–463.
22. Cuony P, Marending M, Alexander DTL, Bocaard M, Bugnon G, Despeisse M, Ballif C. Mixed-phase p-type silicon oxide containing silicon nanocrystals and its role in thin-film silicon solar cells. *Applied Physics Letter* 2010; **97**: 213502-1–213502-3.

23. Wang YH, Lin J, Huan CHA. Multiphase structure of hydrogenated amorphous silicon carbide thin films. *Materials Science and Engineering* 2002; **B95**: 43–50.
24. Kim SH, You DJ, Park JH, Lee SE, Lee HD, Kim D. Front contact layer of multiphase silicon-carbon in thin film silicon solar cell. *Applied Physics Letters* 2012; **101**: 133910-1–133910-3.
25. Veneri PD, Mercaldo LV, Usatti I. Silicon oxide based n-doped layer for improved performance of thin film silicon solar cells. *Applied Physics Letters* 2010; **97**: 023512-1–023512-3.
26. Yamamoto K, Nakajima A, Yoshimi M, Sawada T, Fukuda S, Suezaki T, Ichikawa M, Koi Y, Goto M, Meguro T, Matsuda T, Kondo M, Sasaki T, Tawada Y. A high efficiency thin film silicon solar cell and module. *Solar Energy* 2004; **77**: 939–949.
27. Buehlmann P, Bailat J, Domine D, Billet A, Meillaud F, Feltrin A, Balif C. In situ silicon oxide based intermediate reflector for thin-film silicon micromorph solar cells. *Applied Physics Letters* 2007; **91**: 143505-1–143505-3.
28. Bugnon G, Feltrin A, Bartlome R, Strahm B, Bronneberg AC, Parascandolo G, Ballif C. Microcrystalline and micromorph device improvements through combined plasma and material characterization techniques. *Solar Energy Materials and Solar Cells* 2011; **95**: 134–137.
29. Yamamoto K, Yoshimi M, Tawada Y, Okamoto Y, Nakajima A. Thin film Si solar cell fabricated at low temperature. *Journal of Non-Crystalline Solids* 2000; **266–269**: 1082–1087.
30. Banerjee A, Guha S. Study of back reflectors for amorphous silicon alloy solar cell application. *Journal of Applied Physics* 1991; **69**: 1030–1035.
31. Heo YH, You DJ, Lee H, Lee S, Lee HM. ZnO:B back reflector with high haze and low absorption enhanced triple-junction thin film Si solar modules. *Solar Energy Materials and Solar Cells* 2014; **122**: 107–111.
32. Kluth O, Loffl A, Wieder S, Beneking C, Appenzeller W, Houben L, Rech B, Wagner H, Hoffmann S, Waser R, Anna Selvan JA, Keppner H, Texture etched Al-doped ZnO: a new material for enhanced light trapping in thin film solar cells, *Photovoltaic Specialists Conference*., *Conference Record of the Twenty-Sixth IEEE* 1997; 619–622.
33. Faÿ S, Dubail S, Kroll U, Meier J, Ziegler Y, Shah A. Light trapping enhancement for thin-film silicon solar cells by roughness improvement of the ZnO front TCO, *Proceedings of the 16th European Photovoltaic Solar Energy Conference and Exhibition* 2000; 361–364.
34. Faÿ S, Feitknecht L, Schluchter R, Kroll U, Vallat-Sauvain E, Shah A. Rough ZnO layers by LP-CVD process and their effect in improving performances of amorphous and microcrystalline silicon solar cells. *Solar Energy Materials and Solar Cells* 2006; **90**: 2960–2967.
35. Faÿ S, Steinhauser J, Nicolay S, Ballif C. Polycrystalline ZnO:B grown by LPCVD as TCO for thin film silicon solar cells. *Thin Solid Films* 2010; **518**: 2961–2966.
36. Strahm B, Howling AA, Sansonnens L, Ch Hollenstein, Kroll U, Meier J, Ellert Ch, Feitknecht L, Ballif C. Microcrystalline silicon deposited at high rate on large areas from pure silane with efficient gas utilization. *Solar Energy Materials and Solar Cells* 2007; **91**: 495–502.
37. Carlson D, Arya RR, Bennett M, Chen LF, Jansen K, Li YM, Newton J, Rajan K, Romero R, Talenti D, Twesme E, Willing F, Yang L, Commercialization of multijunction amorphous silicon modules, *Conference Record of the 25th IEEE Photovoltaic Specialists Conference* 1996; 1023–1028.
38. Golay S, Meier J, Dubail S, Kroll U, Shah A. Laser scribing of p-i-n/p-i-n "Micromorph" (a-Si:H/μc-Si:H) tandem cells, *16th EC Photovoltaic Solar Energy Conference* 2000; 494–497.
39. Staebler DL, Wronski CR. Optically induced conductivity changes in discharge produced hydrogenated amorphous silicon. *Journal of applied physics* 1980; **51**: 3562–3268.
40. Terakawa A, Shima M, Isomura M, Tanaka M, Kiyama S, Tsuda S, Matsunami H. Effect of the optical gap on the temperature dependence of a-SiGe solar cell stability. *Journal of Non-Crystalline Solids* 1998; **227–230**: 1267–1271.